Redox-reforming based, integrated solar-natural gas plants: reforming and thermodynamic cycle efficiency

Elysia J. Sheu and Ahmed F. Ghoniem*

Department of Mechanical Engineering, Massachusetts Institute of Technology, 77 Massachusetts Avenue, Cambridge, MA, USA

Abstract

As demand for energy continues to rise, the concern over the increase in emissions grows, prompting much interest in using renewable energy resources such as solar energy. However, there are numerous issues with using solar energy including intermittancy and the need for storage. A potential solution is the concept of hybrid solar-fossil fuel power generation. Previous work has shown that utilizing solar reforming in conventional power cycles has higher performance compared to other integration methods. Most previous studies have focused on steam or dry reforming and on specific component analysis rather than a systems level analysis. In this article, a system analysis of a hybrid cycle utilizing redox reforming is presented. Important cycle design and operation parameters such as the oxidation temperature and reformer operating pressure are identified and their effect on both the reformer and cycle performance is discussed. Simulation results show that increasing oxidation temperature can improve reformer and cycle efficiency. Also shown is that increasing the amount of reforming water leads to a higher reformer efficiency, but can be detrimental to cycle efficiency depending on how the reforming water is utilized.

Keywords: Hybrid Solar-Fossil Fuel, System Analysis, Solar Reforming,

*Corresponding Author: ghoniem@mit.edu, Tel: +1 6172532295, Fax: +1 6172535981

Nomenclature

Latin Letters

HRSG	Heat Recovery Steam Generator	
ΔH^o	Standard Enthalpy of Reaction	kJ/mol
$X_{input,solar}$	Input Solar Share	
Q	Heat Input	W
I	Solar Irradiance	W/m^2
A	Solar Collector Area	m^2
T	Temperature	K
$\tilde{C}$	Mean Flux Concentration Ratio	suns
$\dot{n}$	Molar Flow Rate	mol/s

Greek Letters

σ	Stefan-Boltzmann Constant	$W/m^2/K^4$
η	Efficiency	

Subscripts

red	Reduction
oxd	Oxidation
$solar$	Solar Field Input

$fuel$	Fuel Input
ref	Reformer
rec	Solar Receiver
$chem$	Chemical

1. Introduction

With the expected rise in energy demand and the concern over the concurrent increase in emissions, there has been much interest in the use of renewable resources such as solar energy in power generation. However, in the near term, renewable energy sources, more specifically nonhydropower renewables such as solar and wind energy, are projected to contribute a small fraction of the world's electricity generation, while traditional fossil fuels, such as coal and natural gas are expected to grow [1].

One reason for the slow growth in the use of nonhydropower renewable energy sources is the intermittency and the difficulty with implementing economically viable storage methods. One potential solution for this problem is the idea of hybrid solar-fossil fuel power generation, whose advantages include: 1) the reduction of emissions when compared to fossil fuel only plants and potential reduction of costs when compared to solar only plants, 2) the compatibility with large scale power plants that can be integrated into the existing power grid, and 3) it can be implemented in new plants or as a retrofit.

Within this concept of hybrid solar-fossil fuel power plants, there are three schemes: 1) solarized gas turbine, 2) solar steam integration, and 3) solar reforming [2]. A schematic of these schemes is shown in Figure 1. In the solarized gas turbine, solar energy is used to preheat the compressed air before combustion. For the solar

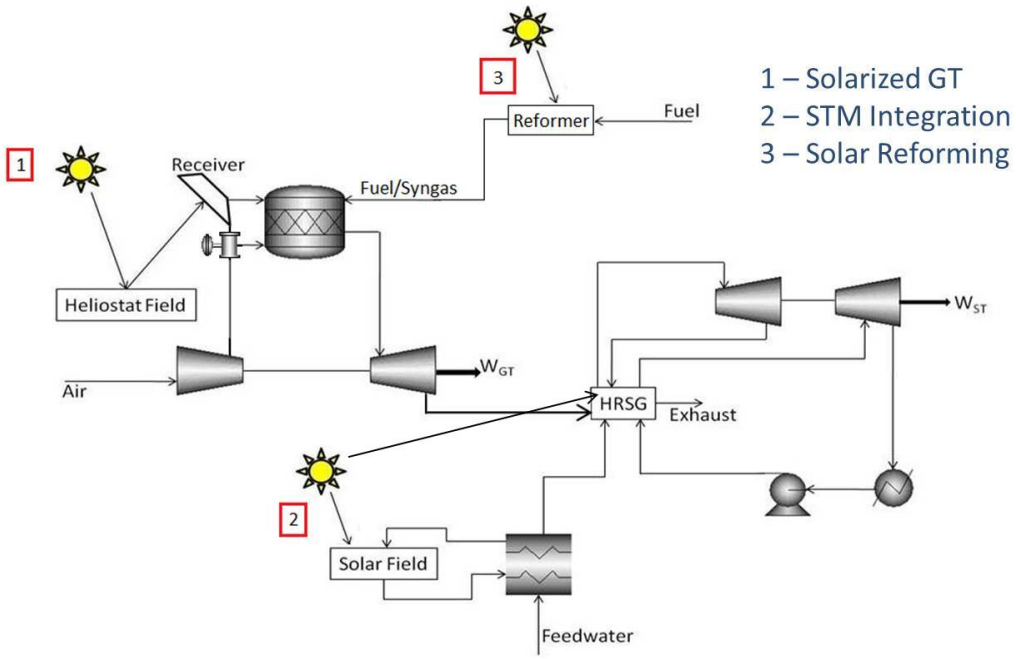

Figure 1: Three Main Hybridization Schemes for Solar-Fossil Fuel Power Cycles

steam integration, the solar energy is used to create additional steam that is used in a steam cycle. The solar reforming approach involves using the solar energy to reform the fuel (natural gas) into syngas (which has a higher heating value) which is then used as a fuel for the gas turbine. The various hybridization schemes have been extensively reviewed in [2].

Comparison among these different hybridization schemes has shown that solar reforming utilizes the solar energy more efficiently [3]. In addition, solar reforming is also a storage mechanism because it stores the solar energy in the form of a chemical fuel [4, 5, 6]. Furthermore, system of a direct expansion chemical cycle utilizing steam reforming of methane shows that CO_2 emissions can be reduced by as much as 22% when compared to traditional combustion of methane [7].

The most common processes proposed for solar reforming are steam reforming, CO_2 (dry) reforming, and to a lesser extent, metal redox reforming. The key reactions for the three processes are shown below:

Steam Reforming:

$$CH_4 + H_2O(v) \rightarrow CO + 3H_2 \quad \Delta H^o = 205\text{kJ/mol [8]}$$

Dry Reforming:

$$CH_4 + CO_2 \rightarrow 2CO + 2H_2 \quad \Delta H^o = 246\text{kJ/mol [8]}$$

Metal Redox Reforming:

$$MO + CH_4 \rightarrow M + CO + 2H_2 \text{ (Endothermic)}$$

$$M + H_2O(v) \rightarrow MO + H_2 \text{ (Exothermic or Endothermic)}$$

where M/MO represents the metal/metal oxide pair chosen for the redox reactions.

For the metal redox reforming, the oxidation step is done with steam. Oxidation with steam can be either endothermic or exothermic depending on the metal/metal oxide pair. Moreover, oxidation with steam yields additional hydrogen. Table 2 shows the enthalpy of reaction for the reduction and oxidation steps for various metal/metal oxide pairs. Metal oxides can have a number of different oxidation states. In Table 2, the oxidation state used is the one most commonly formed/used in metal/metal oxide redox cycles [9].

Depending on the amount of water used in steam reforming or if water is used within the reduction reaction of redox reforming, the water-gas shift reaction can also be a key reaction:

$$CO + H_2O(v) \rightarrow CO_2 + H_2 \quad \Delta H^o = -41\text{kJ/mol [8]}$$

Metal/Metal Oxide	ΔH^o_{red} **[kJ/mol]**	ΔH^o_{ox} **[kJ/mol]**
Cu/CuO	120.40	85.77
Ni/NiO	204.03	2.125
Zn/ZnO	314.79	-108.63
W/WO_3	245.30	-39.14
Fe/Fe_3O_4	243.93	-37.77
Mn/MnO_2	68.34	-18.19
V/V_2O_5	274.45	-68.29

Table 2: Enthalpy of Reaction Values for the Reduction and Oxidation Reactions with Different Metal/Metal Oxide Pairs

The water-gas shift reaction affects the composition of the reformate, which in turn affects the hybrid cycle performance. The effect of the water-gas shift (i.e., using excess water) on both reforming conditions and hybrid cycle performance will be investigated in this paper. For practical operation, often times steam reformers are operated at high steam to methane ratios (between 2:1 and 3:1) in order to prevent coke formation (i.e., thermal cracking of hydrocarbon) [10].

As mentioned previously, solar reforming has been shown to utilize the solar energy more efficiently than the other two schemes. There has been much work on the solar reformer system, but less so on the hybrid system analyses. Moreover, while there have been many studies on steam/dry reformers (either system level or specific reformer component studies) [11, 12, 13, 14, 15, 16, 3, 17], there has not been as much work done on redox reformers. For specifically redox type reformers, there has been an experimental study on a solar reformer combines Zn production methane reforming [18]. There has also been an experimental study on a fixed bed redox reformer investigating using redox reforming with a number of different metal/metal oxide pairs [19]. Moreover, a solar reforming system utilizing redox reforming with iron/magnetite has been proposed and studied in [20]. However, as mentioned previously, these studies are specific reformer studies rather than a hybrid

system level analysis.

In this paper, a system level analysis of a hybrid redox reformer power cycle is performed, and the effect of the pressure, water-fuel ratio, metal oxide, reformer temperature, and the solar energy fraction on the redox reformer performance and the cycle efficiency will be presented. Moreover, the operating conditions for metal redox reforming processes are discussed.

2. Metal Redox Reforming

Metal redox reforming involves a two step process. First, a fuel (methane) is used to reduce a metal oxide, forming metal (or a reduced state of a metal oxide) and syngas. Next, the reduced metal is oxidized using oxygen (air) or steam. Essentially a chemical looping process is created. Only steam oxidation is considered in this analysis. With steam oxidation, the reaction is less exothermic than air oxidation and can even be endothermic depending on the metal. The concept of chemical looping has not only been applied to reforming but also suggested/examined for combustion and other thermochemical processes such as gasification and water splitting [21, 22]. Different metal/metal oxide pairs can be used in a metal redox reforming system. The three most common metals used in chemical looping are copper, nickel, and iron [21], besides Tungsten (W) and Vanadium (V) [19]. The reduction and oxidation reactions for these metal/metal oxide pairs are shown in Table 3.

The enthalpies of reaction were calculated using the enthalpies of formation found in [23]. In essence, the redox reforming is just splitting the steam reforming into two different reactions, and if the two reactions are combined, the overall reaction is the steam reforming reaction. For iron, tungsten, and vanadium, the highest oxidation state is shown as this is the oxide formed during steam oxidation [24, 19]. The oxidation state affects how much oxygen is available for reduction per unit mass of

Metal	Reduction/Oxidation Reactions
Copper	$CuO + CH_4 \rightarrow Cu + CO + 2H_2 \quad \Delta H^o = 120.40 kJ/mol$
	$Cu + H_2O(v) \rightarrow CuO + H_2 \quad \Delta H^o = 85.77 kJ/mol$
Nickel	$NiO + CH_4 \rightarrow Ni + CO + 2H_2 \quad \Delta H^o = 204.03 kJ/mol$
	$Ni + H_2O(v) \rightarrow NiO + H_2 \quad \Delta H^o = 2.125 kJ/mol$
Iron	$\frac{1}{4}Fe_3O_4 + CH_4 \rightarrow \frac{3}{4}Fe + CO + 2H_2 \quad \Delta H^o = 243.93 kJ/mol$
	$\frac{3}{4}Fe + H_2O(v) \rightarrow \frac{1}{4}Fe_3O_4 + H_2 \quad \Delta H^o = -37.77 kJ/mol$
Tungsten	$\frac{1}{3}WO_3 + CH_4 \rightarrow \frac{1}{3}W + CO + 2H_2 \quad \Delta H^o = 245.30 kJ/mol$
	$\frac{1}{3}W + H_2O(v) \rightarrow \frac{1}{3}WO_3 + H_2 \quad \Delta H^o = -39.14 kJ/mol$
Vanadium	$\frac{1}{5}V_2O_5 + CH_4 \rightarrow \frac{2}{5}W + CO + 2H_2 \quad \Delta H^o = 274.45 kJ/mol$
	$\frac{2}{5}V + H_2O(v) \rightarrow \frac{1}{5}V_2O_5 + H_2 \quad \Delta H^o = -68.29 kJ/mol$

Table 3: Reduction and Oxidation Reactions for Different Metal/Metal Oxide Pairs

the metal oxide, and the higher the oxidation state, the more oxygen is available for reduction. Moreover, as mentioned previously, excess water may be added to the reduction reaction to promote the water-gas shift reaction and form extra hydrogen, which would also affect the equilibrium of the reduction reaction. The effect of adding excess water to the reduction step on the hybrid cycle performance will be examined further later.

In order to determine the most appropriate metal/metal oxide pair, the impact of the temperature on equilibrium conversion of the methane and the metal should be examined first.

2.1. Reduction Reaction

For the reduction reaction, methane conversion as a function of temperature is shown in Figure 2. Equilibrium methane conversion is determined using the equi-

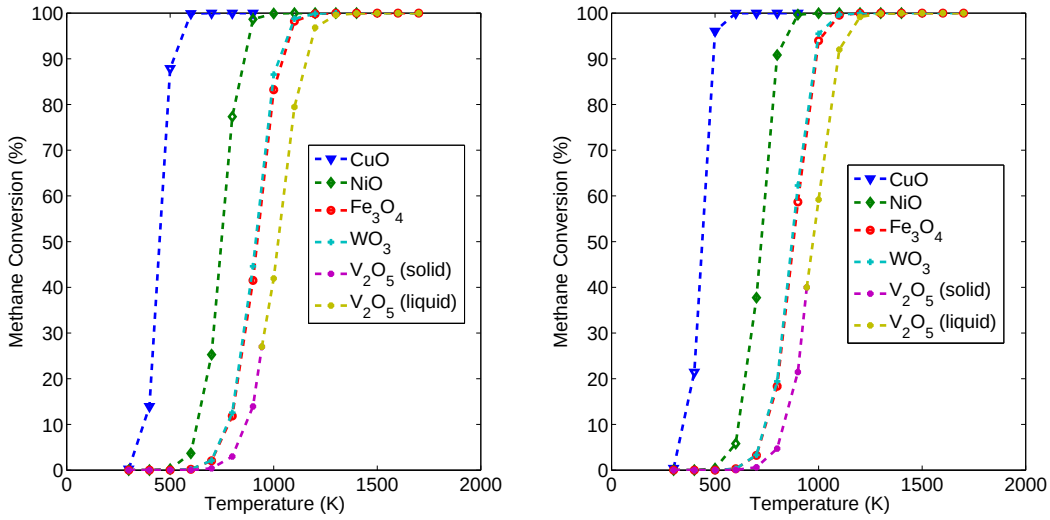

Figure 2: Equilbrium Methane Conversion for CuO, NiO, Fe_3O_4, WO_3, and V_2O_5 for Stoichiometric Metal Oxide to Fuel Ratio (Left) and 2 x Stoichiometric Metal Oxide to Fuel Ratio (Right) (Phase Change for V_2O_5 occurs at approximately 1000 K)

librium constants (Table 4) calculated on the basis of Gibbs free energy of reaction values found in [23]. From Figure 2, it can be seen that reduction of copper oxide requires the lowest temperatures while that of vanadium oxide requires the highest temperatures for near complete conversion. Since the reforming temperature is limited by the solar collector/concentrator system, lower operating temperatures would be preferred. Vanadium oxide melts at approximately 1000 K and therefore may not be appropriate for this reforming process. Figure 2 also shows that increasing the metal oxide to fuel ratio can greatly decrease the temperatures required for complete conversion. While this would increase material cost, it helps decrease solar collector costs and should be considered.

Other considerations when choosing the metal oxide oxygen carrier are the cost

Temperature (K)	**K_p (CuO)**	**K_p (NiO)**	**K_p (Fe_3O_4)**	**K_p (WO_3)**	**K_p (V_2O_5)**
300	6.23e-8	1.99e-22	8.66e-30	6.10e-30	5.05e-35
400	1.26e-2	1.75e-13	4.13e-19	3.39e-19	5.21e-23
500	22.41	4.71e-8	1.22e-12	1.13e-12	9.96e-16
600	3.56e3	2.07e-4	2.69e-8	2.73e-8	7.74e-11
700	1.38e5	8.64e-2	3.49e-5	3.86e-5	2.51e-7
800	2.17e6	8.16	7.56e-3	9.09e-4	1.10e-4
900	1.86e7	283.85	0.49	0.64	0.0126
1000		4.87e3	13.74	19.29	.51
1100		4.99e4	212.96	310.99	9.77
1200		3.47e5	2.10e3	3.13e3	114.20
1300		1.78e6	1.46e4	2.20e4	908.82
1400		7.21e6	7.67e4	1.16e5	5.35e3
1500			3.21e5	4.90e5	2.47e4
1600			1.12e6	1.74e6	9.37e4
1700			3.36e6	5.14e6	3.03e5

Table 4: Equilibrium Constants of the Reduction Reactions (Phase Change for V_2O_5 at approximately 1000 K)

and oxygen carrying capacity. The oxygen carrying capacity affects how much metal/metal oxide is needed. A smaller amount of metal might be advantageous cost wise; however, a larger may be advantageous for transporting heat between the receiver reformer and the power island. Figure 3 shows the oxygen carrying capacity and price of the different metal/metal oxide pairs. While V has the highest oxygen carrying capacity by a wide margin, it is also one of the highest prices. Fe has the lowest price and the second highest oxygen carrying capacity. The oxygen carrying capacity of Cu, Ni, and W are relatively similar, but both Ni and W cost significantly more than Cu.

The pressure dependence of methane conversion in the reduction reaction is shown in Figure 4. The pressure dependence is plotted at different temperatures since the temperatures required for significant methane conversion vary across the different

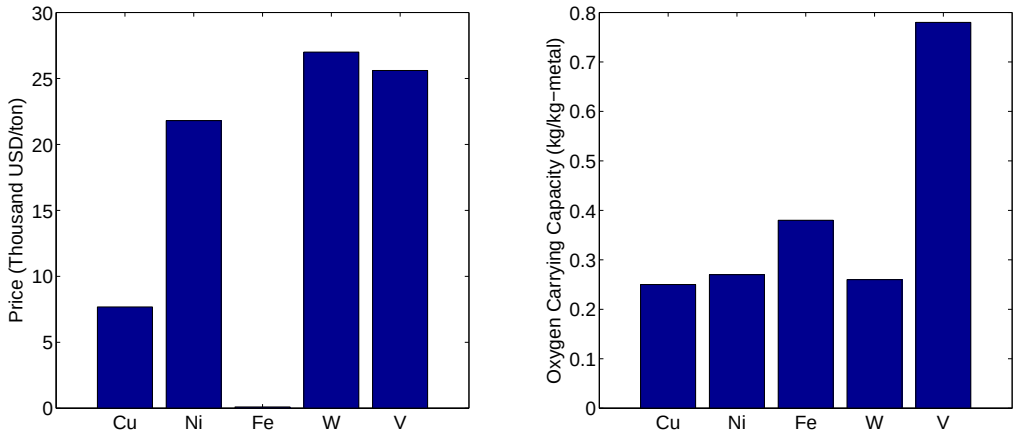

Figure 3: Price (Left) and Oxygen Carrying Capacity (Right) of Different Metals [9]

metal oxides. In other words, if the reforming temperature is high enough such that significant conversion is achieved, then changing the pressure does not have much effect. Similar to steam reforming, lower pressures are favored for methane conversion. However, a steep drop is initially observed, suggesting that the reduction reaction of the redox reforming process is more greatly affected by higher pressures. Nevertheless, the effect of pressure on methane conversion is similar for all the metal/metal oxide pairs.

In addition to these single metal oxides, there has been interest in using bimetallic oxides including nickel, zinc, copper, and cobalt ferrites [25, 26]. Studies have shown that using bimetallic oxides can lead to faster kinetics, higher quality syngas, and decreased carbon formation [25, 26]. The reduction reactions for these bimetallic oxides are

$$\frac{1}{4}\mathrm{CuFe_2O_4} + \mathrm{CH_4} \rightarrow \frac{1}{4}\mathrm{Cu} + \frac{1}{2}\mathrm{Fe} + \mathrm{CO} + 2\mathrm{H_2} \quad \Delta H^o = 92.57\mathrm{kJ/mol}$$

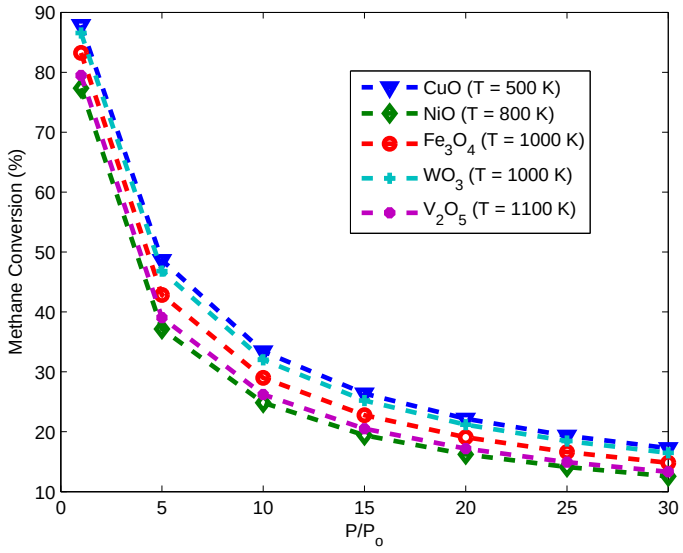

Figure 4: Equilibrium Methane Conversion for CuO, NiO, Fe_3O_4, WO_3, and V_2O_5

$$\frac{1}{4}\mathrm{CoFe_2O_4} + \mathrm{CH_4} \rightarrow \frac{1}{4}\mathrm{Co} + \frac{1}{2}\mathrm{Fe} + \mathrm{CO} + 2\mathrm{H_2} \quad \Delta H^o = 236.29\mathrm{kJ/mol}$$
$$\frac{1}{4}\mathrm{NiFe_2O_4} + \mathrm{CH_4} \rightarrow \frac{1}{4}\mathrm{Ni} + \frac{1}{2}\mathrm{Fe} + \mathrm{CO} + 2\mathrm{H_2} \quad \Delta H^o = 234.61\mathrm{kJ/mol}$$
$$\frac{1}{4}\mathrm{ZnFe_2O_4} + \mathrm{CH_4} \rightarrow \frac{1}{4}\mathrm{Zn} + \frac{1}{2}\mathrm{Fe} + \mathrm{CO} + 2\mathrm{H_2} \quad \Delta H^o = 340.83\mathrm{kJ/mol}$$

Figure 5 shows methane conversion using the original ferrite (magnetite) and the doped ferrites, calculated using the equilibrium constants (Table 5) calculated from Gibbs free energy of reaction found in [23].

Figure 5 shows that, for the most part, doped ferrites yield higher conversion than magnetite, with the only exception being Zn-ferrite. Moreover, Zn-ferrite has a very low melting temperature ($\sim$ 1000 K) and therefore cannot reach complete conversion before it melts. Ni-ferrite and Cu-Ferrite also have a relatively low melting temperature ($\sim$ 1200 K and $\sim$ 1300 K, respectively).

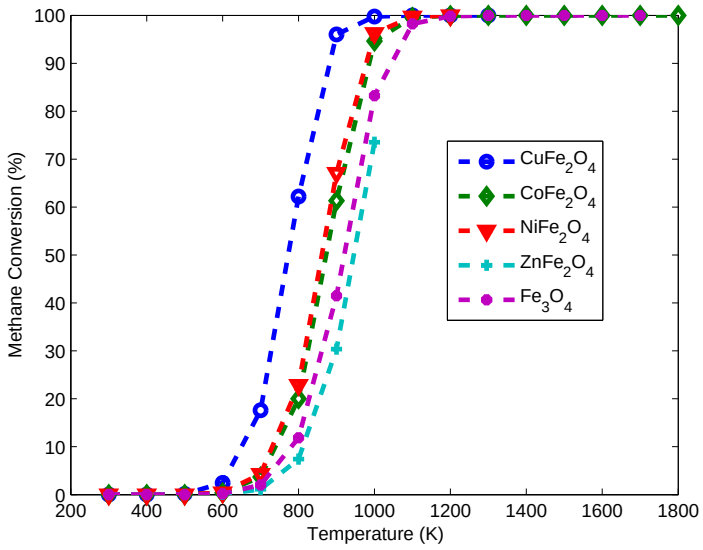

Figure 5: Equilibrium Methane Conversion for Doped ferrites and Magnetite at Stoichiometric Metal Oxide to Fuel Ratios

Based on the different aspects considered: cost, temperatures required, and oxygen carrying capacity, and metal oxide phases, copper, nickel, iron, Cu-ferrite, and Co-ferrite will be investigated further.

2.2. Oxidation Reaction

For the oxidation reaction, the main goal is to convert all of the metal to metal oxide (and producing hydrogen when water is used). Metal oxidation results are shown in Figure 6, determined using the equilibrium constants (Table 6) calculated from the Gibbs free energy of reaction found in [23]. Figure 6 shows that Cu and Ni can not be oxidized into CuO and NiO using steam, respectively, at any reasonable temperatures. Also shown in Figure 6, because the oxidation of Fe favors lower temperatures the oxidation reaction with Fe is exothermic. In addition, super-

Temperature (K)	K_p ($CuFe_2O_4$)	K_p ($CoFe_2O_4$)	K_p ($NiFe_2O_4$)	K_p ($ZnFe_2O_4$)
300	3.58e-23	2.83e-23	6.05e-28	5.46e-32
400	3.96e-14	6.30e-18	1.15e-17	1.00e-20
500	1.22e-8	1.19e-11	1.99e-11	6.85e-14
600	5.98e-5	1.97e-7	3.16e-7	2.71e-9
700	0.026	2.10e-4	3.30e-4	5.49e-6
800	2.55	0.040	0.062	1.77e-4
900	89.08	2.39	3.67	0.16
1000	1.54e3	63.12	96.09	6.00
1100	1.58e4	925.97	1.39e3	
1200	1.10e5	8.70e3	1.30e4	
1300	5.71e5	5.78e4		
1400		2.92e5		
1500		1.18e6		
1600		3.99ee6		
1700		1.17e7		
1800		3.02e7		

Table 5: Equilibrium Constants for Mixed Metal Oxide Reduction Reaction

stoichiometric amounts of water allow for complete conversion of Fe over a wider range of temperatures, which is important as operating temperatures are likely to be higher in order for the reactions to proceed at a reasonable rate.

Furthermore, there is no pressure dependence for the metal oxidation reaction since the number of moles of gas remains constant.

For the mixed metals, Cu-ferrite and Co-ferrite, the oxidation reactions are as follows

$$\frac{1}{4}\mathrm{Cu} + \frac{1}{2}\mathrm{Fe} + \mathrm{H_2O} \rightarrow \frac{1}{4}\mathrm{CuFe_2O_4} + \mathrm{H_2} \quad \Delta H^o = 113.59\mathrm{kJ/mol}$$

$$\frac{1}{4}\mathrm{Co} + \frac{1}{2}\mathrm{Fe} + \mathrm{H_2O} \rightarrow \frac{1}{4}\mathrm{CoFe_2O_4} + \mathrm{H_2} \quad \Delta H^o = -30.13\mathrm{kJ/mol}$$

Based on equilibrium, a comparison between the metal conversion as a function of temperature of the mixed metals and the original metal (Fe) is shown in Figure

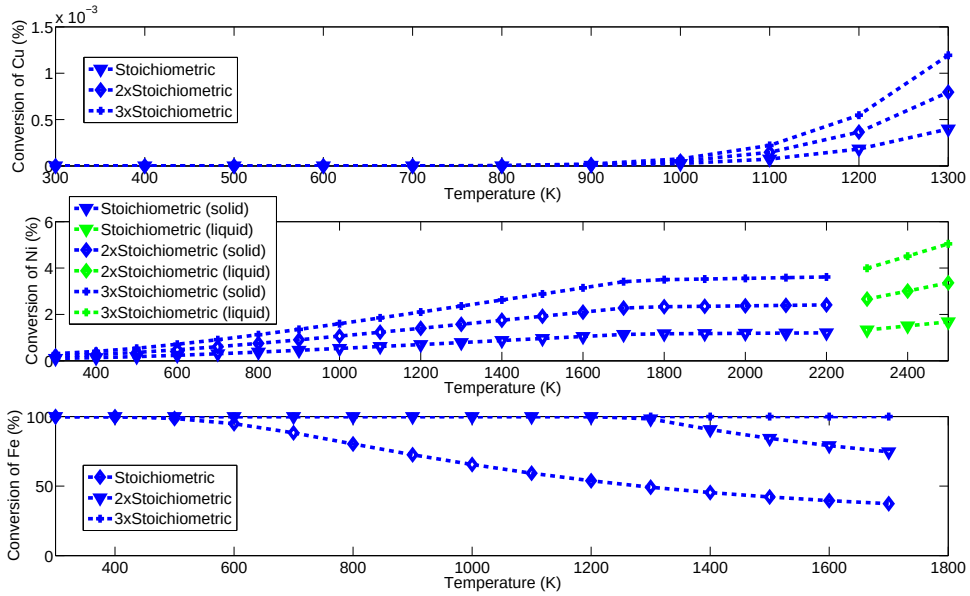

Figure 6: Equilibrium Metal Oxidation Using Steam for Cu (Top), Ni (Middle), and Fe (Bottom) (Jump in Ni Plot Indicates Phase Change)

7. The metal conversion is calculated based on equilibrium constants (Table 7) calculated using Gibbs free energy of reaction found in [23].

From Figure 7, it can be seen that similar to pure copper and nickel, mixed metal of copper and iron cannot be oxidized by steam at sufficiently low temperatures. Also, from Figure 7, the equilibrium metal oxidation conversion is higher for the pure iron than the mixed metal of cobalt and iron.

Based on these results, it seems that either the iron/magnetite pair or the cobalt and iron/cobalt ferrite would be most appropriate for this particular methane/steam redox reformer. There is a tradeoff between the two metal/metal oxide pairs in that the Co-ferrite requires lower temperatures for reduction as compared to the

Temperature (K)	**K_p (Cu)**	**K_p (Ni)**	**K_p (Fe)**
300	3.27e-18	1.02e-3	2.35e4
400	1.90e-14	1.36e-4	576.54
500	3.79e-12	1.80e-3	69.47
600	1.39e-10	2.39e-3	18.36
700	1.91e-9	3.05e-3	7.54
800	1.42e-8	3.77e-3	4.07
900	6.92e-8	4.54e-3	2.64
1000	2.52e-7	5.36e-3	1.90
1100	7.37e-7	6.20e-3	1.45
1200	1.83e-6	7.06e-3	1.16
1300	3.98e-6	7.94e-3	0.97
1400		8.82e-3	0.83
1500		9.70e-3	0.73
1600		0.0105	0.65
1700		0.0115	0.60
1800		0.0118	
1900		0.0119	
2000		0.0120	
2100		0.0121	
2200		0.0122	
2300		0.0135	
2400		0.0153	
2500		0.0171	

Table 6: Equilibrium Constants at Different Temperatures for Oxidation Reaction (Phase Change for Ni at 2300 K)

magnetite, but the mixed cobalt and iron cannot be oxidized with steam as well as the pure iron. For the analysis herein, the iron/magnetite pair is chosen.

To summarize, various metal/metal oxide pairs can be utilized within an redox reforming system. In terms of methane conversion, the reduction reaction prefers higher temperatures and lower pressures while the oxidation reaction can favor either higher or lower temperatures depending on the metal used. Iron/Magnetite is chosen as the metal/metal oxide pair for the system analysis herein due to the temperatures

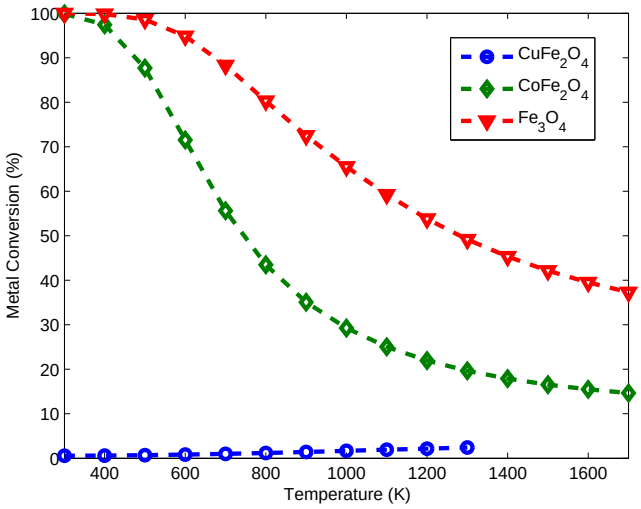

Figure 7: Equilibrium Metal Oxidation Conversion for Doped Ferrites and Magnetite

required for the reactions, material costs, and oxygen carrying capacity. Overall, for the reduction of magnetite, higher temperatures and lower pressures are preferred while for the oxidation of iron with steam, lower temperatures are preferred. Now that a metal/metal oxide pair has been chosen, the hybrid cycle model used for analysis will now be discussed.

3. Hybrid Power Cycle Model

The hybrid power cycle contains two main parts: the solar reforming system and the power cycle. A schematic of the hybrid cycle is shown in Figure 8. A combined cycle with a triple pressure heat recovery steam generator (HRSG) is used. For the system analysis, the redox reformer system is modeled as two separate reactors with the iron/magnetite/Alumina/Ar circulating between the two reactors. The Alumina support flow rate is chosen such that the metal is 60% of the total

Temperature (K)	K_p ($CuFe_2O_4$)	K_p ($CoFe_2O_4$)
300	5.69e-3	719.79
400	6.02e-3	37.79
500	6.9e-3	7.13
600	8.25e-3	2.51
700	9.94e-3	1.25
800	0.012	0.77
900	0.014	0.54
1000	0.017	0.41
1100	0.020	0.33
1200	0.022	0.28
1300	0.025	0.24
1400		0.22
1500		0.20
1600		0.18
1700		0.17

Table 7: Equilibrium Constants for the Mixed Metal Oxidation Reactions

metal/support mass. Ar is used as the carrier gas. The reforming steam is generated within the HRSG. The reformer outlet (including the syngas product as well as the iron/magnetite/Alumina/Ar mixture) is cooled by using the reformer outlet stream to create additional steam for the steam cycle. After cooling, the syngas is sent to the combustor and the solid/carrier gas mixture is sent to the oxidation reactor. In addition, the energy released in the oxidation reactor (reaction is exothermic) is used to create additional steam for the steam cycle. The methane input is kept the same for all simulations. For the redox reformer cycle, water is condensed from the exhaust of the HRSG in order to recycle the water needed for reforming. Table 8 shows the operating parameters of the hybrid cycle.

Two values for the metal oxide flow rate are chosen: almost stoichiometric and twice stoichiometric metal oxide to fuel ratios. Slightly more metal oxide than required is used to represent the fact that in practical operation not all metal oxide is

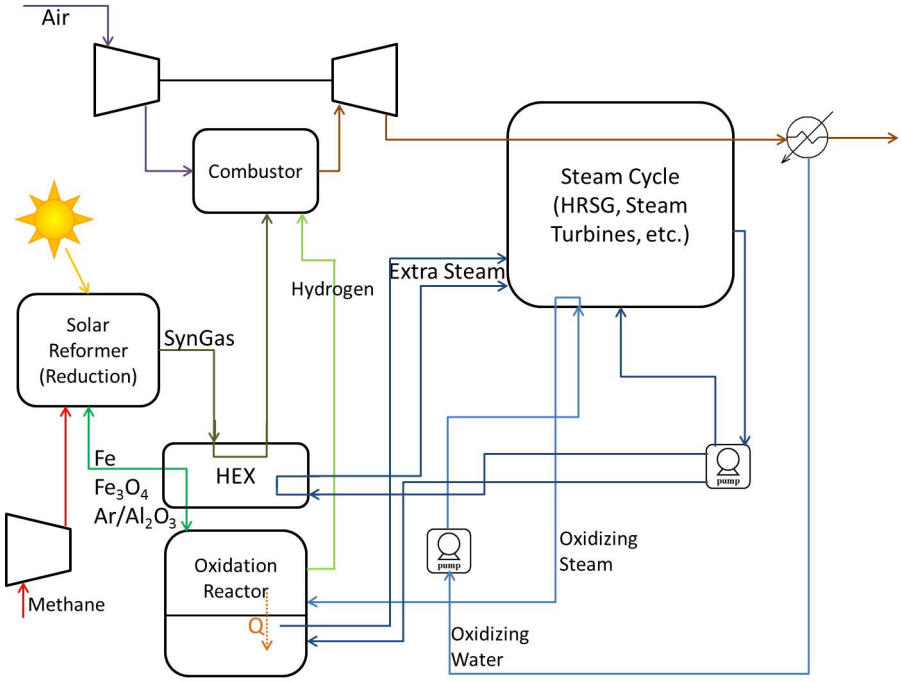

Figure 8: Schematic of Iron Redox Reforming Cycle

available for the reforming process. The alumina support and carrier gas flow rates are adjusted accordingly for the two different cases.

All reformers are modeled as equilibrium reactors where the outlet composition is calculated based on the minimization of Gibbs free energy. No pressure drop is taken into account within the reformer as the pressure drop will depend greatly on the exact design of the reformer system. The absence of pressure drop means that the simulation results will be slightly higher than expected. Also, since the reformer model is based on equilibrium, no validation with experimental reformer studies is performed.

Cycle components such as compressors and turbines are modeled using an isentropic efficiency (value used shown in Table 8). Combustion is assumed to be com-

Parameter	Value(s)
Methane Input	0.125 kmol/s
Gas Turbine Inlet Temperature	1600 K
HRSG High Pressure	85 bar
High Pressure Steam Temperature	700 K
HRSG Intermediate Pressure	25 bar
Intermediate Pressure Steam Temperature	600 K
HRSG Low Pressure	5 bar
Low Pressure Steam Temperature	500 K
Isentropic Efficiency - Turbine	95%
Isentropic Efficiency - Compressor	90%
Metal Oxide Flow Rate	0.032 or 0.064 kmol/s
Alumina Support Flow Rate	0.0484 or 0.105 kmol/s
Carrier Gas Flow Rate (Ar)	0.281 or 0.631 kmol/s
Steam Cycle Flow Rate	0.35 - 0.9 kmol/s
Air Flow Rate	2.5 - 4.0 kmol/s
Reforming Steam	0.128, 0.25, or 0.375 kmol/s
Combustor/Reformer Pressure	10, 20, or 30 bar
Oxidation Reactor Temperature	500, 700, 800, or 820-970 K
Reduction Reactor Temperature	700 - 1100 K

Table 8: Operating Conditions for Hybrid Cycle

plete and adiabatic. The steam cycle flow rate is determined by pinch points within the HRSG for each pressure section. The pinch points are set to 5 K. The gas turbine inlet temperature is fixed at 1600 K by varying the air flow rate into the combustor.

The reforming system is operated at an elevated pressure (combustor pressure). As discussed before, the reforming process prefers lower pressures in terms of methane conversion. However, it is better to operate the reformer at the same pressure as the combustor to avoid having to compress the syngas. It takes much less energy to compress the liquid water and fuel before they are sent to the reformer/turned into steam. There is a potential tradeoff with respect to the operating pressures of the combustor: higher combustor pressure produces more work but affects the conversion of methane in the reformer since the reduction reaction for the metal redox system

favors lower pressures. This trade off will be studied further to determine how exactly pressure affects both reformer and hybrid cycle performance.

The solar collector system is modeled as a single heat source. For the iron redox reforming cycle, solar heat is only supplied to the reduction reformer (and determines the reduction temperature) as the oxidation reformer reaction is exothermic and does not require an external heat source to proceed.

The cycle is modeled in Aspen Plus. How this cycle model is analyzed and the simulation results will be presented next.

4. System Analysis Results

The hybrid cycle is simulated over a range of input solar shares. The "input solar share" is defined as

$$X_{input,solar} = \frac{\dot{Q}_{solar}}{\dot{Q}_{solar} + \dot{Q}_{fuel}}$$

where $\dot{Q}_{fuel}$ is the fuel input into the hybrid cycle and $\dot{Q}_{solar}$ is the solar energy input into the hybrid cycle. $\dot{Q}_{solar}$ is the total amount of solar energy available (before taking into account any receiver or reforming losses) and is defined as

$$\dot{Q}_{solar} = IA$$

where I is the solar irradiance (in W/m^2) and A is the solar collector area.

The solar irradiance I is fixed at 600 W/m^2 for this analysis. Typical design solar shares range between 10% and 30% [2]. Note that this input solar share is merely for a certain design hour, and the actual value changes throughout the day/year. The actual solar share will be less than the design solar share.

The overall reformer performance can be defined as

$$\eta_{ref} = \eta_{rec}\eta_{chem}$$

where η_{ref} is the overall reformer system efficiency, η_{rec} is the receiver efficiency which is based on the solar collector/receiver system used, and η_{chem} is the reformer "chemical" efficiency which is based on how the solar energy is used within the reforming process.

The receiver efficiency is defined as [27]

$$\eta_{rec} = 1 - \left(\frac{\sigma T^4}{I\tilde{C}} \right)$$

where σ is the Stefan-Boltzmann constant, T is the receiver temperature (reformer temperature), and $\tilde{C}$ is the mean flux concentration ratio. This receiver efficiency is based on assuming that the receiver reformer is a black body and that heat losses are mainly due to radiation [27]. $\tilde{C}$ is expressed in the units of "suns" and can vary between 30 and 100 suns for trough systems, between 500 and 5000 suns for tower systems, and between 1000 and 10000 suns for dish systems [27]. For the analysis herein, the solar collector system is assumed to be a tower system with a $\tilde{C}$ of 2500 suns.

The receiver efficiency is dependent on the reformer temperature. Thus, while higher reformer temperatures allow for higher methane conversion (as discussed previously) and can increase the "chemical" efficiency and thus the overall reformer efficiency, it leads to a lower receiver efficiency (i.e., more heat losses) which will adversely affect the overall reformer efficiency.

Based on this receiver efficiency the amount of solar energy actually used in the reforming process is

$$\dot{Q}_{rec} = \eta_{rec} \dot{Q}_{solar}$$

where η_{rec} and $\dot{Q}_{solar}$ are as defined previously.

For this analysis, the chemical efficiency for the redox reformer is calculated based on enthalpy (i.e., heating value) as this "extra" enthalpy gained is the main purpose

of the solar reformer. The redox reformer efficiency is defined as

$$\eta_{chem} = \frac{-\dot{n}_p \Delta H_p|_{T_p} + \dot{Q}_{oxd}}{-\dot{n}_r \Delta H_r|_{T_r} + \dot{Q}_{rec}}$$

where $\Delta H_p|_{T_p}$ and $\Delta H_r|_{T_r}$ is the enthalpy of the reformer products and reactants at product temperature T_p and reactant temperature T_r, respectively.

The hybrid cycle performance will be evaluated based on the overall first law cycle efficiency. The cycle efficiency is defined as

$$\eta_{cycle} = \frac{\dot{W}_{hybrid}}{\dot{Q}_{fuel} + \dot{Q}_{solar}}$$

where $\dot{W}_{hybrid}$ is the work output from the hybrid cycle.

The effect of pressure, reforming water, metal oxide, oxidation temperature, and solar share on the redox reformer and hybrid cycle performance will now be discussed.

4.1. Effect of Amount of Metal Oxide Used

The iron redox cycle is simulated for a range of solar shares using approximately stoichiometric metal oxide and twice the stoichiometric amount. The reforming water for oxidation is adjusted accordingly. The pressure for the reformer/combustor is set to 20 bar. The oxidation temperature is set to 500 K. Figure 9 shows the reformer efficiency for the two cases over a range of solar shares. The methane conversion and reformer temperature for the two cases are also plotted in Figure 9 for reference.

As can be seen from Figure 9, the reformer efficiency is higher in the 2 x stoichiometric case. This is mainly due to the fact that there is more mass circulating through the reformer leading to more energy released in the oxidation reactor resulting in better reformer efficiency. Moreover, the receiver efficiency is higher for the 2 x stoichiometric case because, as shown in Figure 9, it has a lower reforming temperature which also leads to a higher overall reformer efficiency. Although the reforming temperature is higher in the stoichiometric case, these gains from the higher

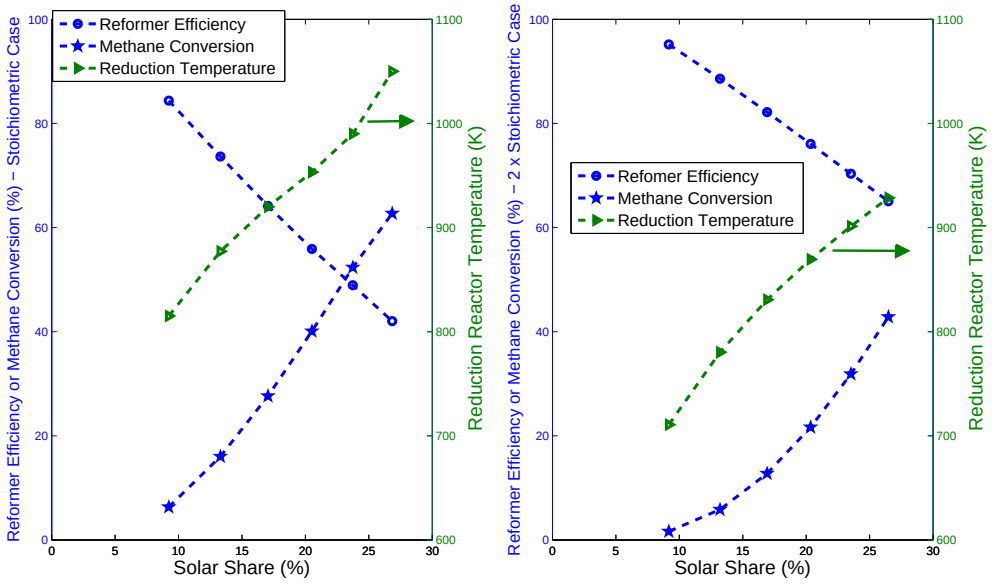

Figure 9: Reformer Efficiency, Temperature, and Methane Conversion for Stoichiometric Metal Oxide (Right) and 2 x Stoichiometric Metal Oxide (Left) (T_{oxd} = 500 K)

reforming temperature (i.e., more methane conversion) are unable to overcome the higher receiver losses and lower amount of heat released from the oxidation reaction (due to the lower mass). Moreover, as solar share increases, the reformer efficiency decreases. This is because the lowering receiver and chemical efficiency with the higher solar share. The receiver efficiency drops with the solar share rise because of the higher reforming temperature at higher solar share. The chemical efficiency decreases because the rate of increase in reforming gains (i.e., more methane conversion and more energy released from oxidation reactor) is not the same as the rate of increase in the solar energy added at higher solar share. In other words the rise in the reforming temperature at higher solar share is not enough to raise the reforming gain.

Figure 10 shows the cycle efficiency for the two cases. From Figure 10 it can

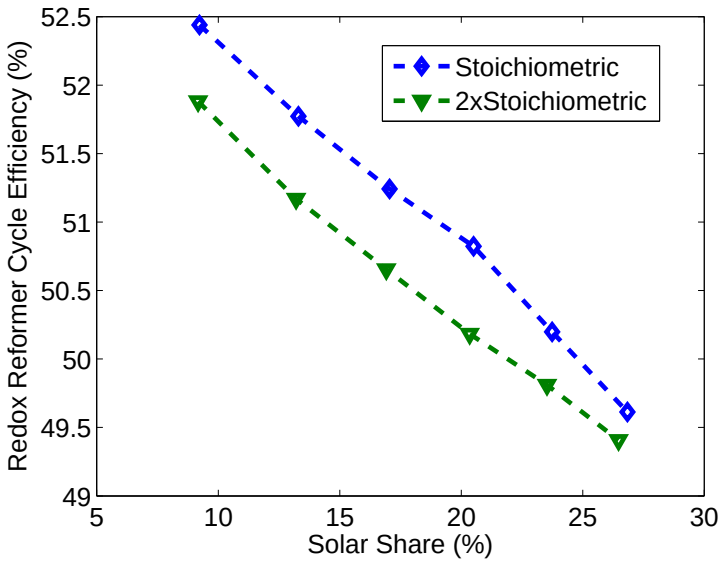

Figure 10: Cycle Efficiency for Stoichiometric Metal Oxide and 2 x Stoichiometric Metal Oxide

be seen that the stoichiometric case has a higher cycle efficiency even though the 2 x stoichiometric case has a higher reformer efficiency. The reforming temperature is higher in the stoichiometric case which although not necessarily beneficial to the reforming efficiency, it is beneficial to the cycle efficiency because the cycle gain from the higher reforming temperature in the stoichiometric case is sufficient enough to counteract the reforming losses. The cycle efficiency decreases with increasing solar share, and this trend is due to the decreasing reformer efficiency with increasing solar share.

Overall, increasing the metal oxide to fuel ratio increases the reformer efficiency but decreases the cycle efficiency. Next, the effect of the oxidation temperature will be investigated.

4.2. Effect of Oxidation Temperature

As discussed previously, the oxidation reaction being exothermic favors lower temperatures. However, with larger amounts of reforming water (higher than stoichiometric) the oxidation temperature can be raised and complete conversion can still be achieved (as discussed previously). The higher oxidation temperature can potentially be beneficial for both the reformer and cycle performance. To determine the effect of oxidation temperature on reformer and cycle performance, the redox reformer cycle is simulated using three different oxidation temperatures: 500 K, 700 K, 800 K. In addition, the performance of the redox cycle using solar heat in the reduction reactor only is compared to the case of using solar energy in the reduction and oxidation reactors. The reforming water flow rate is set to 0.250 kmol/s (approximately twice the stoichiometric amount), stoichiometric amount of metal oxide is used, and the combustor/reformer pressure is set to 20 bar.

4.2.1. 500 K, 700 K, and 800 K Cases

Figure 11 shows that at very low solar shares, the low oxidation temperature case (500 K) has a similar or higher reforming efficiency than the higher oxidation temperature cases. With higher oxidation temperature, the oxidation reaction is less exothermic (which means less energy release and lower reformer efficiency). At low solar shares, the reforming temperatures are low. While a higher reduction reactor temperature (700 and 800 K) yields a higher methane conversion (due to higher reactor temperature - see Figure 12), these gains are not able to overcome the low energy release from the oxidation reactor which leads to the lower reformer efficiency. As the solar share increases, the higher reforming temperature leads to higher chemical efficiency and higher reformer efficiency (despite lower receiver efficiency). At 700 K, despite the low oxidation temperature, (and therefore lower reforming temperature

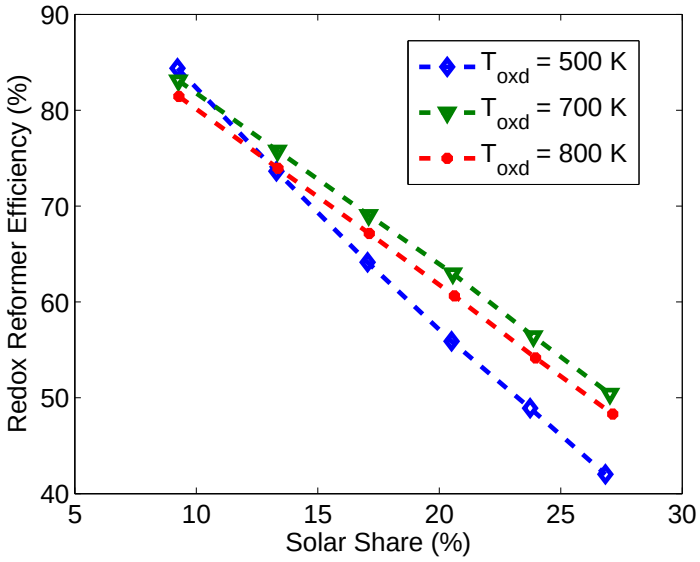

Figure 11: The Reformer Efficiency at Different Oxidation Temperatures

- see Figure 12) it has a higher reformer efficiency. The increase in conversion (see Figure 12) in the 800 K case (which is beneficial to the chemical efficiency) is not large enough to counteract the lower energy release in the oxidation reactor at the higher oxidation temperature (800 K). Thus the chemical efficiency is higher at 700 K which leads to the higher overall reformer efficiency.

Figure 13 shows the redox cycle efficiency for different oxidation temperatures. Somewhat different from the reformer efficiency comparison, the cycle efficiency improves with the oxidation temperature. Despite the fact that higher oxidation temperatures may be detrimental to the reformer efficiency, the higher temperature is preferred for the cycle efficiency. Again, the cycle efficiency decreases with increasing solar share due to the decreasing reformer efficiency.

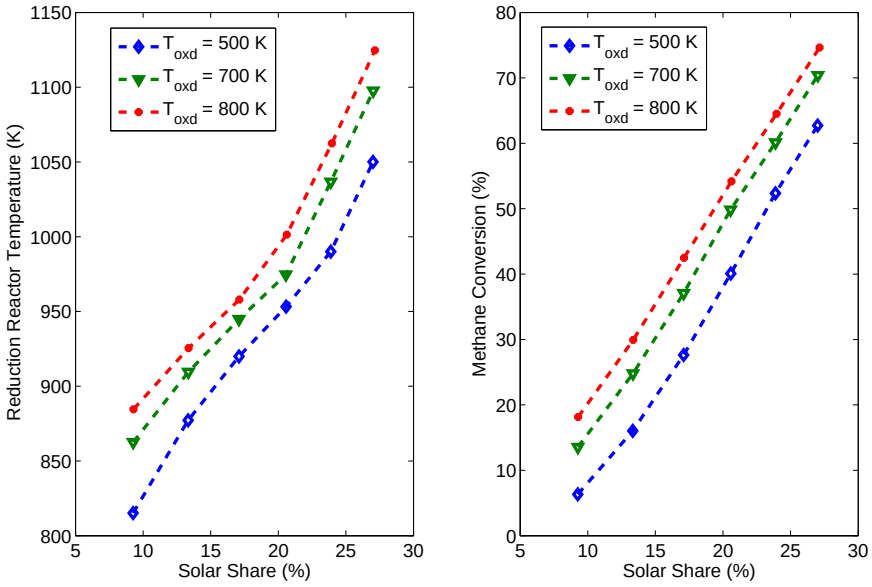

Figure 12: Reformer Temperature and Methane Conversion at Different Oxidation Temperatures

4.2.2. Using Solar in Both Reduction and Oxidation Reactor for High Oxidation Temperatures

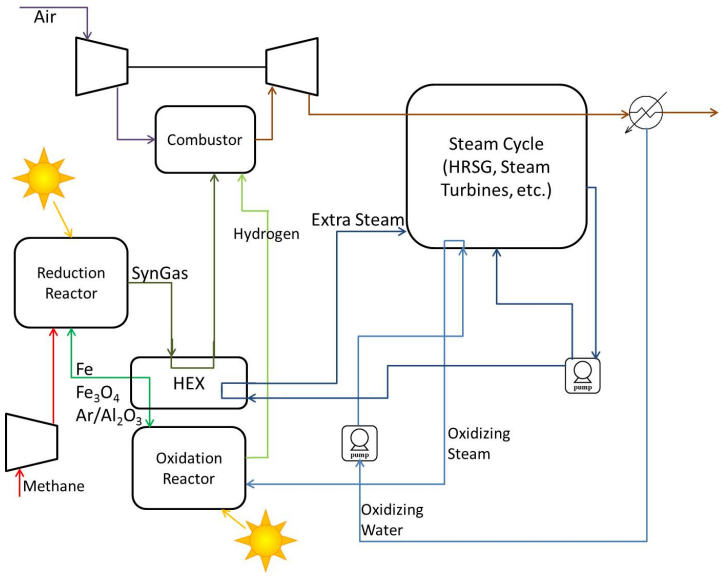

Figure 14: Redox Cycle with Both Oxidation and Reduction Reactors utilizing Solar Energy

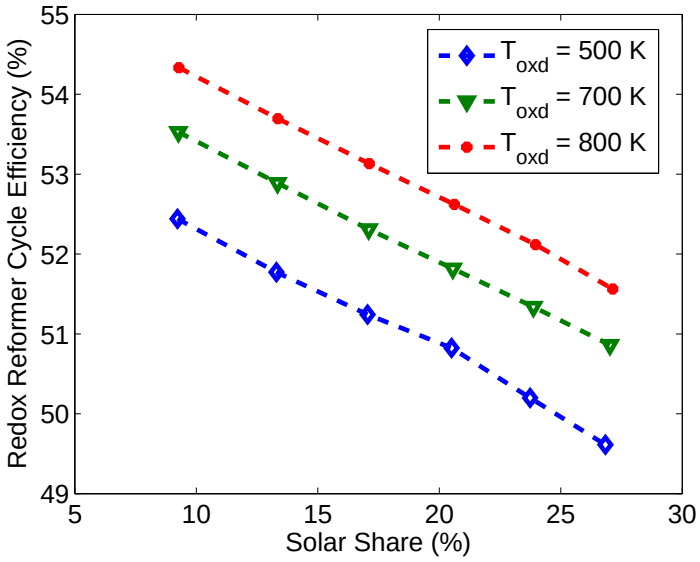

Figure 13: Cycle Efficiency at Different Oxidation Temperatures

At oxidation temperatures significantly higher than 800 K, the oxidation reaction is no longer exothermic due to the heat required for both the reforming steam and the incoming metal/support/carrier gas mixture [24]. Therefore, both the oxidation and reduction reactor should utilize solar energy. The solar input for the oxidation reactor is kept fixed (which yields the 860 - 970 K temperature range) and that for the reduction reactor is varied to simulate different solar shares. The solar input into the oxidation reactor is chosen such that the oxidation reactor temperatures reached are significantly higher than 800 K. The revised schematic of the redox cycle is shown in Figure 14. All other parameters of the cycle are the same as before.

The reformer efficiency for T = 800 K is shown in Figure 15 for reference. When solar energy is used by both reactors there is no heat release from the oxidation reaction and the calculation of the reformer efficiency is adjusted accordingly. Figure

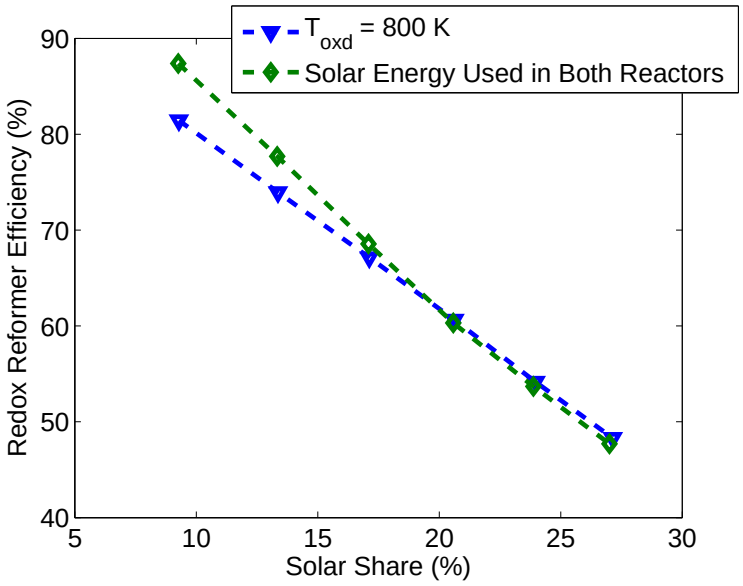

Figure 15: Reformer Efficiency at Different Oxidation Temperatures, Both Reduction and Oxidation Reactor Use Solar Energy (T_{oxd} = 860 - 970 K) and T_{oxd} = 800 K

15 shows that solar energy in both reactors case and the 800 K case have similar reformer efficiencies with the former having slightly higher efficiency at low solar share and slightly lower reformer efficiency at higher solar share. This is because at the same solar share there is less solar energy available for the reduction reactor which leads to lower reduction temperatures/less methane conversion (see Figure 16) in the 860-970 K case (despite the higher inlet temperature due to the higher oxidation temperature). However, in the 860-970 K case, the solar energy is also being used in the oxidation reaction which can help the reformer efficiency.

Figure 17 shows the corresponding cycle efficiency. At lower solar shares, the 800 K case has higher cycle efficiency and then the trend reverses at higher solar share. The cycle efficiency is higher at the lower oxidation temperature (800 K) at low solar share because there is not much solar energy available for the reduction

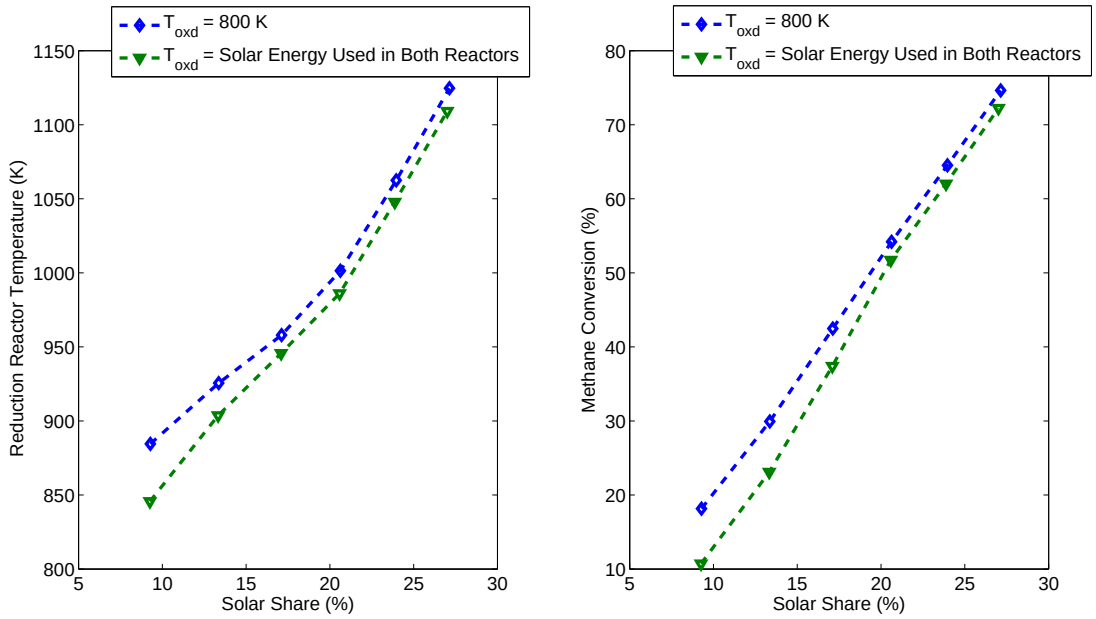

Figure 16: Reformer Temperature and Methane Conversion at Different Oxidation Temperatures (Both Reduction and Oxidation Reactors Use Solar Case and T = 800 K Case)

reactor in the solar energy used in both reactors case which leads to a lower reduction reactor temperature (despite the higher inlet temperature from the higher oxidation temperature). The stream from the reduction reactor into the cycle is at a lower temperature which is detrimental to the cycle performance, and the higher temperature oxidation product stream into the power cycle is not enough to counteract the losses from the lower temperature reduction product stream. For higher solar shares, the solar energy used in both reactors case has a higher cycle efficiency because there is more solar energy available for the reduction reactor.

In summary, for the most part, raising the oxidation reactor temperature improves the reformer and cycle efficiency. The reformer operating pressure effect on performance will be studied next.

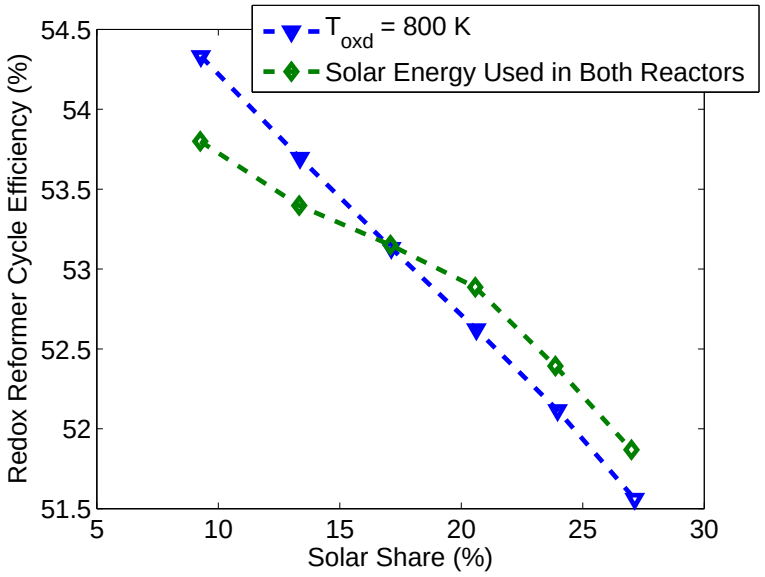

Figure 17: The Cycle Efficiency at Different Oxidation Temperatures, Both Reduction and Oxidation Reactors Use Solar Case (T_{oxd} = 860 - 970 K) and T_{oxd}800 K Case

4.3. Effect of Pressure

To study the effect of pressure on the cycle and reformer efficiency, the hybrid cycle is simulated for three different combustor/reformer operating pressures (10, 20, and 30 bar). Stoichiometric reforming water and metal oxide are used. The oxidation temperature is set to 500 K (in order to achieve complete conversion of metal with stoichiometric amount of reforming water).

The reformer efficiency is plotted in Figure 18, showing that the operating pressure does not significantly affect the reformer efficiency. While higher pressure leads to less reforming (as discussed previously), the higher pressure cases also have higher reforming temperature (see Figure 19) which is beneficial for reforming. The reforming efficiency decreases with increasing solar share.

Figure 20 shows the cycle efficiency for the three different cases, showing that the

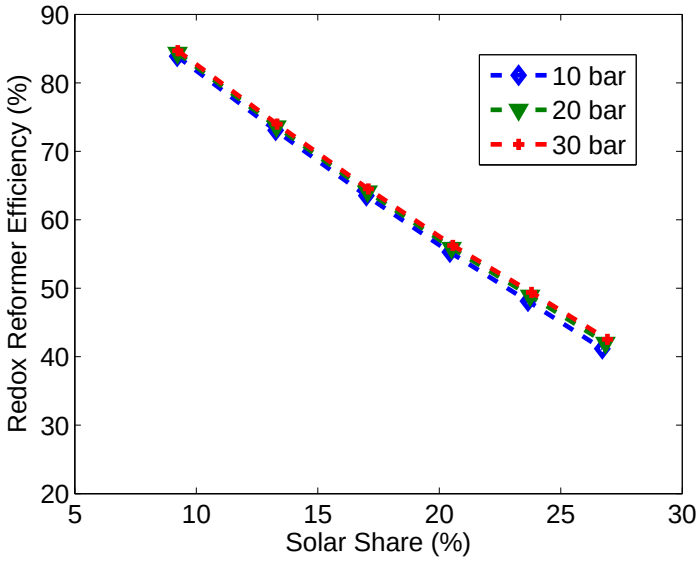

Figure 18: Reformer Efficiency at Different Operating Pressures for Redox Reformer (T_{oxd} = 500 K)

cycle efficiency increases with increasing pressure.

To summarize, raising the operating pressure of the reformer does not affect the reformer efficiency significantly but does improve the cycle efficiency. For these pressure simulations, stoichiometric amount of reforming water is used (.128 kmol/s). However, as discussed before using more than stoichiometric amount of reforming water allows for higher oxidation temperature which can be beneficial to both reformer and cycle performance. Therefore, the effect of the amount of reformer water used is investigated next.

4.4. Effect of Amount of Reformer Water Used

The amount of reforming water used within the hybrid cycle affects the composition of the reformer and the temperature of the oxidation reactor, which impacts

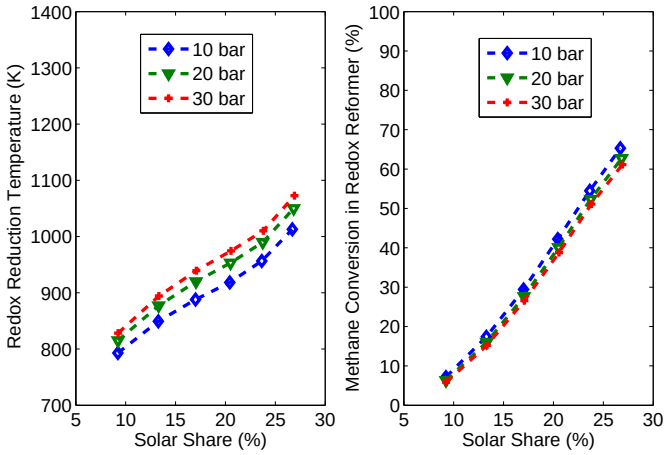

Figure 19: Reformer Temperature (left) and Methane Conversion (right) at Different Operating Pressures for Redox Reformer(T_{oxd} = 500 K)

the reformer and cycle efficiency. The hybrid cycle is simulated with higher than stoichiometric reforming water: 0.25 and 0.375 kmol/s (approximately two times stoichiometric and three times stoichiometric), and the oxidation reactor is operated at a higher temperature. Based on the oxidation temperature study discussed previously, the oxidation reactor utilizes solar energy which leads oxidation temperatures higher than 800 K (the exact range of temperatures depends on the amount of reformer water used). This operating condition is chosen because, as discussed before, this case yields the highest reformer and cycle efficiencies over a larger range of solar shares. For the 0.375 kmol/s case specifically, within the redox reformer cycle, the reforming water can be used entirely within the oxidation reactor or split between the oxidation and reduction reactor (i.e., using 0.25 kmol/s of reforming water in the oxidation reactor and using the rest in the reduction reactor). Both cases will be investigated. For all simulations, the combustor/reformer pressure is set to 20 bar

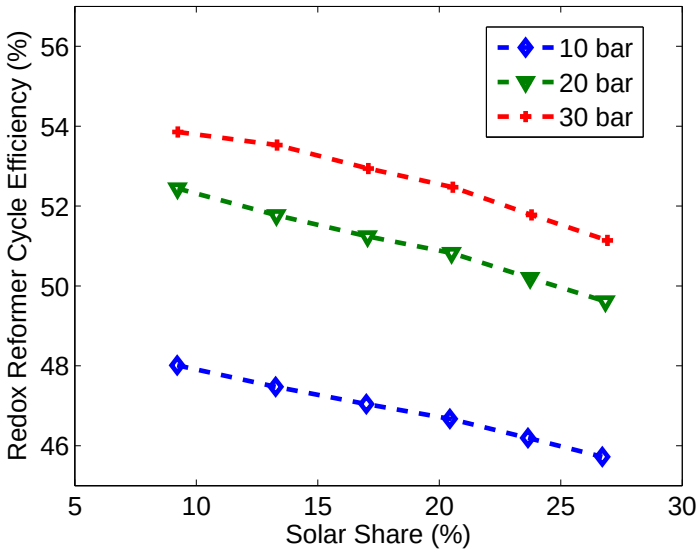

Figure 20: The Hybrid Cycle Efficiency at Different Operating Pressures

and a stoichiometric amount of metal oxide is used.

4.4.1. Reforming Water Used in Oxidation Reactor Only

The reformer efficiency for the two water cases for the redox reformer is shown in Figure 21. Increasing the amount of reforming water raises the reformer efficiency. Since the reforming water is only used in the oxidation reactor, the oxidation temperature changes with the amount of steam used. The 0.375 kmol/s case has a lower range of oxidation temperature which leads to a lower reduction reaction temperature (Figure 22). However, the gains from a higher receiver efficiency (due to the slightly lower reformer temperature) are sufficient to counteract the very little reforming losses of the lower temperature which leads to a higher reformer efficiency.

Figure 23 depicts the cycle efficiency for the two cases, showing that the cycle efficiency does not change much with increasing amounts of reforming water although

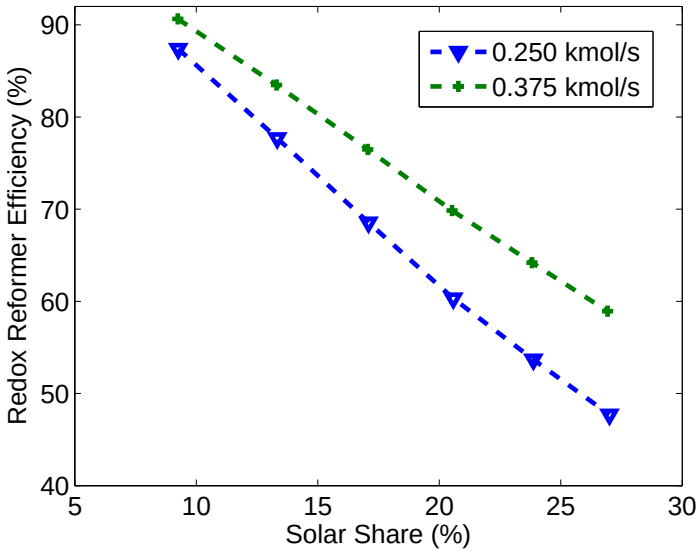

Figure 21: Reformer Efficiency for Different Amounts of Reforming Water for Redox Reformer - Oxidation Reactor Only (T_{oxd} = 860-970 K for 0.250 kmol/s case and T_{oxd} = 820-920 K for 0.375 kmol/s case)

the 0.375 kmol/s case has a higher reformer efficiency. The reason is because although the 0.250 kmol/s case has a lower reformer efficiency, the oxidation temperature is higher (860-970 K vs 820-920 K) which means that the oxidation product stream temperature is higher and the inlet metal oxide stream temperature to the reduction reactor is higher which leads to a slightly higher reduction reactor temperature (Figure 22). These higher temperature streams (both oxidation and reduction product streams) may not necessarily be beneficial to the reformer efficiency (due to lower receiver efficiency), but are beneficial to the cycle efficiency. Moreover, less energy is extracted from the HRSG to create steam because not as much reforming steam is used.

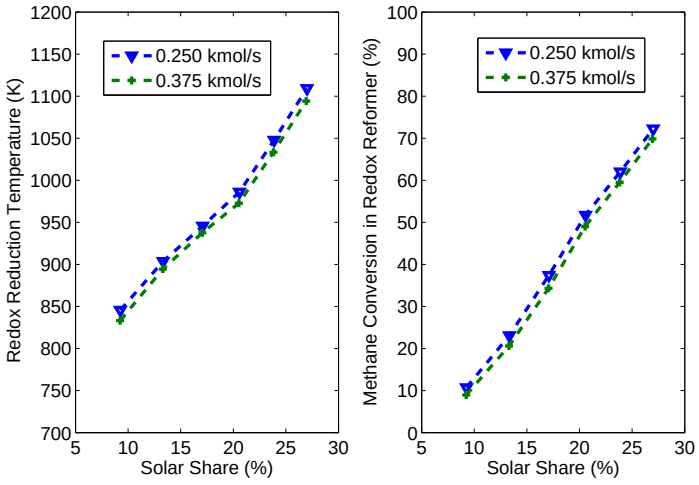

Figure 22: Reformer Temperature and Methane Conversion for Different Amounts of Reforming Water for Redox Reformer - Oxidation Reactor Only (T_{oxd} = 860-970 K for 0.250 kmol/s case and T_{oxd} = 820-920 K for 0.375 kmol/s case)

4.4.2. Reforming Water Used in Oxidation Reactor and Reduction Reactor

The reformer efficiency is shown in Figure 24 with the 0.375 kmol/s case for the redox reformer using reforming water in both the oxidation and reduction reactors. Figure 24 shows that utilizing reforming water in both the oxidation reactor and reduction reactor does not really affect the reformer efficiency. Although for the most part the reduction temperature is lower in the case where reforming water is used in both reactors, the presence of water in the reduction reactor allows for some steam reforming/water-gas shift to occur which allows for more methane conversion. The presence of additional reforming reactions and the higher receiver efficiency due to the lower reforming temperature make up for the higher reformer temperature in the case where reforming water is only used in the oxidation reactor. Again, similar to before, the reformer efficiency is higher for the higher reforming water case.

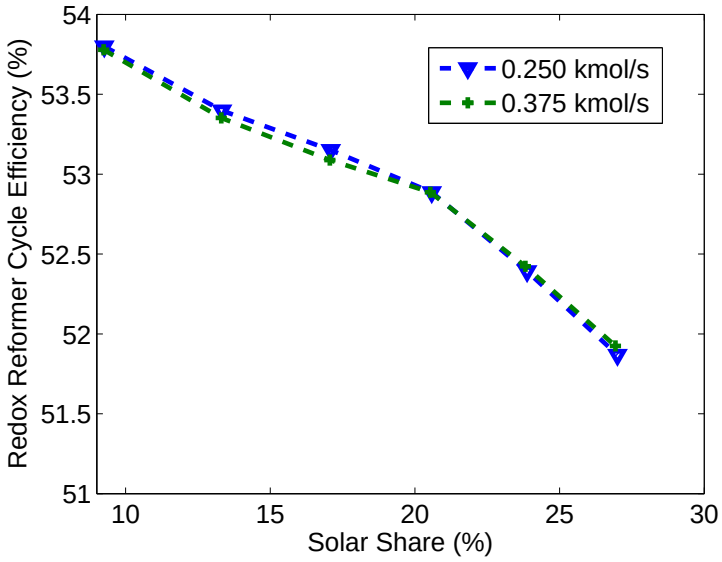

Figure 23: Cycle Efficiency for Different Amounts of Reforming Water for Redox Reformer - Oxidation Reactor Only

Figure 25 shows the cycle efficiency for the different cases. Despite having similar reformer efficiencies, for the 0.375 kmol/s case, the cycle efficiency is lower when the reforming water is used in both reactors. The reason for this is the lower reforming temperatures which leads to a lower temperature stream entering the power cycle which leads to less work output and lower cycle efficiency.

Overall, increasing the amount of reforming water yields a higher reformer efficiency and can increase the cycle efficiency if the reforming water is used in the oxidation reactor only.

5. Conclusion

In summary, the system analysis shows the effect of reformer/combustor pressure, amount of reforming water, amount of metal oxide, and oxidation reaction

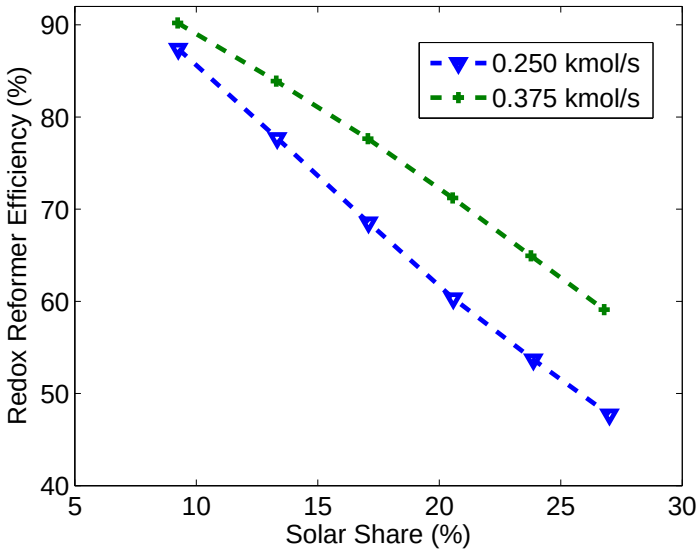

Figure 24: Reformer Efficiency for Different Amounts of Reforming Water for Redox Reformer - Use in Both Oxidation and Reduction Reactor in 0.375 kmol/s case (T_{oxd} = 860-970 K for 0.250 kmol/s case and T_{oxd} = 820-940 K for 0.375 kmol/s case)

temperature on both redox reformer and hybrid cycle performance. (1) Adding more metal oxide to the redox reforming cycle leads to higher reforming efficiency but lower cycle efficiency. (2) Raising the oxidation temperature usually increases the reformer and cycle efficiency. (3) To reach very high oxidation temperatures, both the reduction and oxidation reactors should utilize the solar energy. (4) The higher reformer/combustor pressures does not affect the reformer performance significantly but does lead to better cycle performance. (5) Increasing the amount of reforming water leads to better reforming performance and can lead to lower cycle performance depending on how the reforming water is used within the redox reformer. This system analysis has identified important design and operation aspects of the hybrid redox reformer cycle that can greatly affect performance. Future work

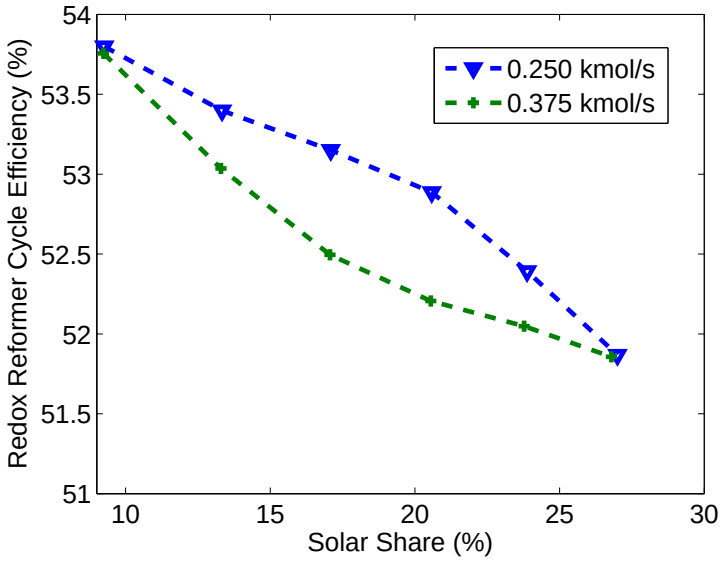

Figure 25: Cycle Efficiency for Different Amounts of Reforming Water for Redox Reformer - Both Oxidation and Reduction Reactor

will include comparing redox reformer and redox reformer cycle performance with the performance of hybrid cycles that utilize the more traditional steam and dry reforming.

Acknowledgment

The authors would like to thank the King Fahd University of Petroleum and Minerals in Dhahran, Saudi Arabia, for funding the research reported in this article through the Center for Clean Water and Clean Energy at MIT and KFUPM under project number R12-CE-10. Aspen Plus® was generously provided by Aspen Technology.

References

[1] International Energy Outlook 2013. Tech. Rep.; U.S. Energy Information Administration; 2013.

[2] Sheu, E.J., Mitsos, A., Eter, A.A., Mokheimer, E.M.A., Habib, M.A., Al-Qutub, A.. A review of hybrid solar-fossil fuel power generation systems and performance metrics. ASME Journal of Solar Energy Engineering 2012;134(4):041006:1–17.

[3] Sheu, E.J., Mitsos, A.. Optimization of a hybrid solar-fossil fuel plant: Solar steam reforming of methane in a combined cycle. Energy 2013;51:193–202.

[4] Kodama, T.. High-temperature solar chemistry for converting solar heat to chemical fuels. Progress in Energy and Combustion Science 2003;29(6):567 – 597.

[5] Steinfeld, A., Weimer, A.W.. Thermochemical production of fuels with concentrated solar energy. Optics Express 2010;18(S1):A100–A111.

[6] Zedtwitz, P., Petrasch, J., Trommer, D., Steinfeld, A.. Hydrogen production via the solar thermal decarbonization of fossil fuels. Solar Energy 2006;80(10):1333 – 1337.

[7] Wagar, W., Zamfirescu, C., Dincer, I.. Thermodynamic analysis of solar energy use for reforming fuels to hydrogen. International Journal of Hydrogen Energy 2011;36(12):7002 – 7011.

[8] Tamme, R., Buck, R., Epstein, M., Fisher, U., Sugarmen, C.. Solar upgrading of fuels for generation of electricity. Journal of Solar Energy Engineering 2001;123(2):160–163.

[9] Yamaguchi, D., Tang, L., Burke, N., Chiang, K., Rye, L., Hadley, T., et al. Hydrogen Energy: Challenges and Perspectives; chap. 2. Intech; 2012, p. 31–54.

[10] Liu, J.A.. Kinetics, catalysis and mechanism of methane steam reforming. Masters Thesis, Worcester Polytechnic Institute; 2006.

[11] Anikeev, V., Bobrin, A., Ortner, J., Schmidt, S., Funken, K.H., Kuzin, N.. Catalytic thermochemical reactor/receiver for solar reforming of natural gas: Design and performance. Solar Energy 1998;63(2):97 – 104.

[12] Berman, A., Karn, R.K., Epstein, M.. Steam reforming of methane on a Ru/Al_2O_3 catalyst promoted with mn oxides for solar hydrogen production. Green Chem 2007;9:626–631.

[13] Buck, R., Muir, J.F., Hogan, R.E.. Carbon dioxide reforming of methane in a solar volumetric receiver/reactor: the CAESAR project. Solar Energy Materials 1991;24(14):449 – 463.

[14] Maria, G.D., Tiberio, C., D'Alessio, L., Piccirilli, M., Coffari, E., Paolucci, M.. Thermochemical conversion of solar energy by steam reforming of methane. Energy 1986;11(8):805 – 810.

[15] Dahl, J.K., Weimer, A.W., Lewandowski, A., Bingham, C., Bruetsch, F., Steinfeld, A.. Dry reforming of methane using a solar-thermal aerosol flow reactor. Industrial & Engineering Chemistry Research 2004;43(18):5489–5495.

[16] Levy, M., Rubin, R., Rosin, H., Levitan, R.. Methane reforming by direct solar irradiation of the catalyst. Energy 1992;17(8):749 – 756.

[17] Wörner, A., Tamme, R.. CO_2 reforming of methane in a solar driven volumetric receiver reactor. Catalysis Today 1998;46(23):165 – 174.

[18] Steinfeld, A., Brack, M., Meier, A., Weidenkaff, A., Wuillemin, D.. A solar chemical reactor for co-production of zinc and synthesis gas. Energy 1998;23(10):803 – 814.

[19] Kodama, T., Ohtake, H., Matsumoto, S., Aoki, A., Shimizu, T., Kitayama, Y.. Thermochemical methane reforming using a reactive WO_3/W redox system. Energy 2000;25(5):411 – 425.

[20] Steinfeld, A., Kuhn, P., Karni, J.. High-temperature solar thermochemistry: Production of iron and synthesis gas by Fe_3O_4-reduction with methane. Energy 1993;18(3):239 – 249.

[21] Adanez, J., Abad, A., Garcia-Labiano, F., Gayan, P., de Diego, L.F.. Progress in chemical-looping combustion and reforming technologies. Progress in Energy and Combustion Science 2012;38(2):215 – 282.

[22] Fan, L.S.. Chemical Looping Systems for Fossil Energy Conversions. John Wiley & Sons Inc.; 2010.

[23] Barin, I., Sauert, F., Schultze-Rhonhof, E., Sheng, W.S.. Thermochemical Data of Pure Substances. VCH Verlagsgesellschaft mbH; 1993.

[24] Stehle, R., Bobek, M., Hooper, R., Hahn, D.. Oxidation reaction kinetics for the steam-iron process in support of hydrogen production. International Journal of Hydrogen Energy 2011;36(22):15125(11).

[25] Kang, K.S., Kim, C.H., Cho, W.C., Bae, K.K., Woo, S.W., Park, C.S.. Reduction characteristics of cufe2o4 and fe3o4 by methane; cufe2o4 as an oxidant for two-step thermochemical methane reforming. International Journal of Hydrogen Energy 2008;33(17):4560 – 4568.

[26] Kodama, T., Shimizu, T., Satoh, T., Nakata, M., Shimizu, K.I.. Stepwise production of co-rich syngas and hydrogen via solar methane reforming by using a Ni(II)ferrite redox system. Solar Energy 2002;73(5):363 – 374.

[27] Steinfeld, A., Meier, A.. Solar fuels and materials. In: in Chief: Cutler J. Cleveland, E., editor. Encyclopedia of Energy. New York: Elsevier; 2004, p. 623 – 637.